Σ
SPE 49321

Implementation of multirate technique to measure relative permeabilities accounting for capillary effects

G.A. Virnovsky, SPE and K.O. Vatne, SPE, Rogaland Research, S.M. Skjaeveland, SPE, Stavanger College, and A. Lohne, Rogaland Research.

This paper was prepared for presentation at the 1998 SPE Annual Technical Conference and Exhibition held in New Orleans, Louisiana, 27–30 September 1998.

Abstract

A practical implementation of the multi-rate steady-state technique to determine relative permeabilities from steady-state floods and its comparison with the standard steady-state technique is the main subject of the paper. The multi-rate technique is based on the theory of two-phase flow, and facilitates analytical corrections of relative permeabilities to account for capillary end effect. This is especially of practical importance if the experiment is performed at low rates when the relative role of capillary forces increases.

Normally, it is recommended to perform flooding experiments at high rates and/or on long cores to suppress capillary effects. Though this approach ensures simplicity in the interpretation procedure it disregards several factors one of which is that the relative permeabilities may depend on the rate. Proper account for capillary effects makes usage of long cores and high rates unnecessary.

A number of steady-state core floods have been performed at different rates varying from a high rate typically used in the lab experiments to a low rate approaching the range of typical reservoir rates. The experimental results, i.e. a set of relative permeabilities depending on the rate, have been interpreted both without and with account for capillary end effect. The previously developed analytical corrections for capillary effects were implemented in the interpretation. The results of analytical interpretation are quality controlled by numerical simulation of the experiments. It is shown that much of the difference observed in relative permeability curves and residual saturations measured at different rates can be explained by the influence of capillary end effect.

Introduction

The steady-state technique is one of conventional methods applied in special core analysis to determine relative permeabilities. Since the classical paper [10] it is recognized that capillary forces significantly affect laboratory experiments though neglected in the standard interpretation procedures. In order to avoid inaccuracies resulting from capillary effects neglect generally 2 options exist: either to avoid them by using sufficiently high total rates (which is not always possible in case of low permeable rocks), or to introduce the corrections taking into consideration capillary pressure. An analytical approach to correct the steady-state measurements of relative permeabilities taking into account capillary forces has been developed and tested against simulated data in [13], [14], [15]. The method employs self-similarity of the steady-state two-phase flow with respect to flow rate. The same idea was used to determine capillary pressure and relative permeability of the non-wetting phase in [9], [6] for a more restricted model, only the non-wetting phase is flowing.

In the present paper the analytical corrections are applied to real experimental data. It is shown how the measured data are corrected step by step using *EXCEL* work sheet.

Experimental planning

To ensure measurable capillary end effects the injection rates for the flooding experiments have to be planned based on the parameters of the core plug, capillary pressure, and the estimates of the unknown relative permeabilities.

Input data. To guide in planning the experiments, simulations of the steady-state experiments have been performed, using the core flood simulator *CENDRA*. Steady-state drainage experiments at 2 different total rates have been simulated.

Capillary pressure was measured by centrifuge method on a plug cut from the same core. The measurements were interpreted by Hassler-Brunner method, see Figure 1. The length of the core is 25 cm. The grid is 150x1x1, of which the 50 blocks close to the core outlet have a length of 1 mm, while the length of the rest is 2 mm. The relative permeabilities functions used in the simulations, see Figure 2, were taken from literature, Ref. [12].

Results

The relative permeabilities back calculated from simulated data by Darcy's law are plotted in Figure 2 together with the curves from the simulator input. At high total rate of 5cc/min the calculated curves are very close to the true counterparts, i. e. there is very little influence of the capillary end effects on the total pressure drop. At total rate of 0.2cc/min the calculated water relative permeability reveal little rate dependence while oil relative permeability curve clearly deviates from its true counterpart The difference between those curves is judged to be sufficiently high to be detected from real measurements subjected to measurement errors.

Based on the above simulation results it was decided to carry out 3 drainage experiments at total rates of 5, 0.2 and 0.5cc/min.

Experimental arrangement

Fluids. Synthetic formation water and n-decane where used in the experiments. Before entering the core, the brine was bubbled with nitrogen gas to displace oxygen and filtered through a 0.45 μm filter.

Apparatus[1]. A schematic of the two-phase flow apparatus is shown in Figure 3. The main parts of the apparatus are a pumping system, a two-phase separator, and a core holder.

The pumping system consists of five computer controlled cylinders that have the capability of recycling two phases simultaneously through a core sample. The cylinders are paired, and two cylinder pairs are used for recycling water and oil (or a gaseous phase). Each phase is pumped into the core sample with accurate and virtually pulse free flow rates. For each of the cylinder pairs, one cylinder delivers fluid into the sample, while the other receive fluid through the return line from the separator. The receiving cylinder runs at a slightly higher rate than the delivering cylinder, which implies that the receiving cylinder is ready to deliver fluid into the sample before the delivering cylinder is empty. By continuously adjusting the rates and the pressures, the take over between the cylinders in one pump can occur smoothly. The fifth cylinder is working in a constant pressure mode, and acts as a back pressure regulator within 50 mbar accuracy. This cylinder is connected to the water return line, but is in contact with both phases indirectly through the separator. It provides an excellent back pressure control, and tracks any leakages that might occur throughout the experimentation. The flow rates are adjustable from 0.001 ml/min to 10 ml/min.

A two-phase separator is used for volume measurements. An acoustic separator is used for separation of produced fluids, and for continuously monitoring the production from the outlet face of the core sample. Two bores are connected to each other, and fluid from the core sample enters in one of the bores at the bottom of the separator, where they are separated. The other bore is the measuring bore, and is connected to the separation bore by two channels, one at the top of the separator and one at the bottom. An acoustic transducer is located in the bottom of the measurement bore. Through measurements of the time for an acoustic wave (generated by the transducer) to echo off the interface between the water and oil phase and a calibration stub, the distance from the transducer to the interface can be determined. From this measurement, the water volume in the separator may be calculated. The static accuracy of the volume determination is $\pm$0.01ml, while the dynamic accuracy is empirically determined to be $\pm$0.07ml. The accuracy is poorer when the oil phase are recycled due to the different rates of the delivering and receiving cylinders in one pump. This involves that cylinder five is compensating for a pressure loss caused by the higher rate of the receiving cylinder. As a consequence the meniscus in the separator will continuously be moving up and down. The shape of the meniscus will change with the direction of movement, and hence a hysteresis effect in the volume measurements will occur. However, by optimizing the return rate the movement of the oil water interface and the hysteresis effect is minimized.

A hydrostatic core holder is used in the apparatus. For steady state experiments the inlet distribution end piece has two separate spiral grooves for water and oil, ensuring distribution of both phases across the entire core inlet face, and a pressure port in the center. The outlet distribution end piece is of conventional type with three concentric rings and cross-hatch every 45 degrees. A wire screen is placed on the outlet distribution end piece to minimize particle washout and to ensure uniform fluid flow across the outlet end face. For unsteady state experiments, both distribution end pieces are of the conventional type. Several rubber washers are placed behind each distribution end piece to transmit an axial stress proportional to the confinement pressure. The core sample is completely covered with Teflon tape, tin foil and a hydrogenated nitrile sleeve.

The pressure drop across the core sample is measured by a high resolution differential pressure transmitter with adjustable range. The maximum range was zero to 7 bar for the high rate test and zero to 320 mbar for the low rate and the medium rate measurements. he accuracy during recirculation is within 1% of the measured value.

The pumps, the separator and the core holder are all placed in a heating cabinet, and provide a closed loop and recycling of both phases up to reservoir conditions (which for this apparatus is 41 MPa and 160°C). The apparatus is capable of running either steady-state type experiments or unsteady-state type experiments, i.e. either one or two phases can be simultaneously injected into the core sample. The monitoring of the apparatus and data acquisition (pressures, volumes, temperature etc.) are automated and performed by a personal computer.

Core test procedure. Three steady-state drainage tests have been performed consequently on a Berea core at three distinct total rates as planned above. The floods have been performed vertically injecting oil downwards.

The test procedure is as follows.

1. Core assembly

2. Miscible cleaning;
3. Saturation with water and measurement of permeability to water
4. Steady state drainage test at a specified rate
5. Measurement of water content by vacuum distillation
6. Repeat steps 2-5 with the next rate planned.
7. Miscible cleaning, drying, helium pore volume measurement

Experimental results. Water-oil primary drainage steady state relative permeabilities were measured on a Berea core at three different total rates. First a high rate test was performed with 300 ml/h total rate, then a low rate test was performed with 12 ml/h total rate, and at last a medium rate test was performed with 30 ml/h total rate.

TABLE 2 displays dimensions, porosity and water permeability of the Berea core measured before each steady state test. The water permeability value increased from 165 m*D* to 216 m*D* during the test program. The respective water permeability measured before each steady state test was used as a reference absolute permeability in the relative permeability calculations.

The measured pressure drop across the core and the average water saturation are presented in TABLE 3 for 3 rates and 9 fractional flows.

Interpretation of experiments

Gravity correction. In the experimental setup with vertical positioning of the core holder the total pressure drop across the core is different from the pressure drop readings due to gravity effect on the fluid inside pressure transducer tubing. In our experiments the transducer tubing was filled with water, which means that only oil pressure drop has to be corrected for gravity.

$$\Delta p_o = \Delta p^m - \Delta\gamma L \qquad (1)$$

The relative permeabilities calculated from the measured data by Darcy's formula including gravity correction (1) are shown in Figure 4.

In the analytical corrections below only the pressure drops are corrected for gravity, while the effect of gravity on the saturation distribution is ignored. According to Ref. [8] this effect is small even for high permeable cores. Gravity effects are fully taken into account in the simulation of the experiments described below.

Analytical corrections to account for capillary end effect in steady-state floods were introduced and verified against simulated data in Refs. [13], [15]. The expressions are as follows:

$$S^0 = \bar{S} + \frac{d\bar{S}}{d\ln q_t}, \qquad (2)$$

$$k_{ri}(S^0) = \tilde{k}_{ri}\left[1 - \frac{d\ln \tilde{k}_{ri}}{d\ln q_t}\right]^{-1}, \quad i = o, w \qquad (3)$$

$$\tilde{k}_{ri} = \frac{u_i L \mu_i}{\Delta p_i k}$$

The correction consists of 2 parts, saturation correction, and relative permeability correction. The corrected value of the relative permeability is calculated from the Equation (3). It corresponds to the saturation at the core inlet, S^0 which is calculated from the Equation (2).

The correction of the saturation is straight forward. It is done according to the Equation (2), as shown in TABLE 4.

To implement the formula for relative permeability correction (3), first it is necessary to obtain the individual phase pressure drop for each of the 2 phases. This is done based on the analysis of the pressure continuity across the core boundaries.

As can be observed from the capillary pressure curve, Figure 1, capillary pressure threshold is zero (or at least insufficient to be measured by centrifuge), thus pressure continuity at the outlet is ensured for both phases. At the inlet of the core, the phase pressure in the non-wetting phase is continuous, while the phase pressure in the wetting phase is discontinuous as explained in Refs. [13], [15]. The inlet end effect was analyzed by way of simulation in Ref. [14]. The discontinuity in the wetting phase pressure at the inlet is caused by the counter-current flow, i.e., rapid imbibition of the wetting phase and simultaneous expulsion of the non-wetting phase from the core into groves of the inlet end piece supplying wetting phase. The non-wetting phase forms a thin layer, a film, attached to the core inlet which creates high resistance for the wetting phase to get through. During the counter-current flow the resistance of the film builds up, and so does the pressure drop in the wetting phase across the film. This process continues until the pressure drop across the film becomes equal to the capillary pressure at the core inlet just inside the core.

At steady state, the measured total pressure drop across the core is therefore equal to the pressure drop in the non-wetting phase (oil). The pressure drop in the wetting phase (water) is smaller than the total pressure drop by the value of capillary pressure at the inlet, which can be obtained from the capillary pressure curve and the saturation at the inlet calculated from Equation (2).

$$\Delta p_w = \Delta p^m - P_c(S^0) \qquad (4)$$

The consequence of operations to calculate the corrections and the results are shown in TABLE 5 and TABLE 6, and Figure 5

and Figure 6.

The resulting relative permeability curves are displayed in Figure 7. By comparison of Figure 4 and Figure 7 one can easily see that capillary corrections have dramatically reduced the difference between relative permeabilities measured at different rates. The low rate curves measured at total rates of 0.2 and 0.5 cc/min after correction for capillary end effect have approached the curves measured at high rate of 5 cc/min.

Simulation.

The experimentally measured data were history matched using the steady-state simulator presented earlier, Ref. [16] facilitating accurate and rapid computation of all the relevant characteristics of steady-state core floods with account for gravitational, capillary and viscous forces. The relative permeabilities may be input either as tables, or as Corey-functions. In the case considered, Corey representation has been found sufficient to reconcile the simulated and measured pressure drops across the core and average saturations. The match obtained between experimental and the simulated data is presented in Figure 9 - Figure 11. The resulting relative permeability curves, see Figure 8, for all three rates exhibit very little difference, similar to the analytical interpretation above.

Discussion

Rate dependence of relative permeabilities

As stated in Ref.[2] on page 92 "The effects of displacement pressure, pressure gradient, and flow rate on the shape of relative permeability curve has long been a controversial subject in petroleum-related literature." Some confusion is introduced due to the fact that in addition to its potential influence on the relative permeabilities the rate definitely influences the capillary end effect. From some of the published data it is not always clear whether those 2 different phenomena are sorted out.

In refs. [7], [5] the results are reported in terms of dimensionless parameter

$$\pi_2 = \frac{\sigma}{\mu u_t} \qquad (5)$$

or similar which is a measure of capillarity dominance over viscous forces. In [7], [5] relative permeability curves both for wetting and non-wetting phase display a tendency to increase as the capillary dominance decreases, i.e., they reveal the same behavior as the curves without capillary corrections shown in Figure 4. The reliability of those results may be argued since the capillary end effect has not been accounted for in either of the referenced papers, since a standard interpretation technique neglecting capillary forces was used. The observed tendency (or part of it) might be the result of the unaccounted end effect. As explained in the Appendix this tendency is a typical manifestation of the end effect.

According to Lake[4] at

$$N_{vc} < 10^{-5}, \quad \text{i.e.} \quad \pi_2 = N_{vc}^{-1} > 10^5 \qquad (6)$$

the residual phase saturations are roughly constant. An extensive study of relative permeability rate dependence has been performed by Skauge *et al*[11]. The experimental results were interpreted by parameter estimation technique which takes into account capillary effects. It has been found that the critical capillary number, N_{vc}, is in the range

$$6*10^{-5} < N_{vc}^{critical} < 10^{-4} \qquad (7)$$

Using the relevant core and fluid properties, the dimensionless criterion at the highest rate of 5cc/min is readily calculated to be $\pi_2|_{5cc/min} = 0.47*10^6$ meaning that in our experiments relative permeabilities should be rate insensitive, since the conditions (6), (7), both are satisfied. This conclusion conforms with our results.

Experimental uncertainties. Some uncertainties are associated with the observed experimental behavior as explained below.

Absolute permeability variation. Absolute permeability of the core measured before each flooding test was not constant. It systematically increased from test to test. This could also mean that other properties of the core, e.g., capillary pressure, could have changed either during the tests or during the core cleaning.

Evolution of average saturation with rate. Evolution of average saturation with increase of total rate in the experiments revealed unexpected behavior. Theoretically, in a strongly water-wet core at a fixed injected fractional flow the average saturation can only decrease. This type of behavior is also seen from simulation, Figure 12. From experiments, see Figure 13, the water saturation increases with rate at high fractional flows, behaves non-monotonically at medium fractional flows, and decreases at low water fractional flows. A possible explanation to this effect is the following.

At low water saturations the flow is dominated by capillary forces at all rates, since capillary pressure magnitude is high, while at higher water saturations the magnitude of capillary pressure decreases, and the regime of the flow changes gradually with rate increase so that relative permeabilities become rate dependent. The condition for rate independence of relative permeabilities, i.e. the threshold above which capillary forces prevail, probably, should be formulated in a different way than in Eq. (6) taking into account the capillary pressure dependence on saturation. The velocity restriction would then be stronger in the regions with low capillary

pressure. The observed saturation behavior indicates indirectly that relative permeabilities are rate dependent.

Acknowledgment

The paper presents the results obtained within the *RESERVE*, the Norwegian research program. The project is sponsored by the Research Council of Norway, Norsk Hydro, Elf Petroleum Norge, Saga Petroleum and Den Norske Shell. The financial support from the sponsors is gratefully acknowledged.

Conclusions

1. To validate the previously developed analytical corrections for relative permeabilities, water-oil drainage steady state relative permeabilities were measured on one Berea core at three different rates.
2. The analytical corrections are implemented to correct the measured relative permeabilities. The accuracy of the corrected relative permeabilities is approximately the same as of those obtained by parameter estimation technique.
3. Rate sensitivity of relative permeabilities has been analyzed based on the measured data. It was found that much of the difference observed in relative permeability curves and residual saturations measured at different rates can be explained by the influence of capillary end effect.

Nomenclature

A = crossection area of the core
f = water fractional flow function
F = injected fractional flow of water
k = absolute permeability
k_r = relative permeability
$\tilde{k}_{ri}$ = quantity defined in Eq. (3)
L = core length
N_{vc} = dimensionless viscous to capillary forces ratio
p = pressure
P_c = capillary pressure
q =fluid rate
S = water saturation
S^0 = water saturation at core inlet
u = fluid velocity
V_p = pore volume
γ= specific gravity
Δ = increment
λ = phase mobility
μ = viscosity
π = dimensionless criterion
σ = interfacial tension
ϕ= porosity

Subscripts

o = oil
t = total
vl =viscous limit
cl = capillary limit
w=water

Superscripts

m = measured

References

1. Guo, Y., Vatne, K.O.: "Use of a new generation recirculation system for steady-state relative permeability measurement." presented at the 7-th European IOR Symposium in Moscow, Russia, October 27-29 1993.
2. Honarpour, M., Koederitz, L., Harvey, A.H.: *Relative permeability of petroleum reservoirs.* CRC Press Inc. 1986.
3. Honarpour, M.M, Huang, D.D., Dogru, A.H.: "Simultaneous measurements of relative permeability, capillary pressure, and electrical resistivity with microwave system for saturation monitoring" SPE 30540, presented at the ATCE Dallas 1995
4. Lake. L.W.: *Enhanced oil recovery.* Prentice Hall , New Jersey, 1989.
5. Lefebvre du Prey, E.J. "Factors affecting liquid-liquid relative permeabilities of a consolidated porous medium." SPE 3039. SPE Journal, Febr. 1973, p. 39-47.
6. Lenormand, R., Eisenzimmer, A., Delaplace, Ph.: "Improvements of the semi-dynamic method for capillary pressure measurements." Presented at the SCA Conference held in San Francisco, USA, 12-14 Sept. 1995.
7. Leverett, M.C. "Flow of oil-water mixtures through unconsolidated sands." *Trans. AIME* **132**, 1939, p.149.
8. Mitlin, V.S., McLennan, J.D., Green, S.G.: "A note on simultaneously determining two phase relative permeability and capillary pressure of porous rocks from steady-state flow experiments: accounting for gravitational forces and fluid compressibility." to be published in *J. of Colloid and Interface Sci.*
9. Ramakrishnan, T.S., Capiello, A.: "A new technique to measure static and dynamic properties of a partially saturated porous medium" *Chem. Eng. Sci.*, **46**, 1991, 1157-1163.
10. Richardson, J.G., Kerver, J.A., Hafford, J.A., and Osoba, J.S.: "Laboratory Determination of Relative Permeability", Trans. AIME, **195** (1952) 187-196.
11. Skauge, A., Haaskjold G., Thorsen, T., Aara, M.: "Accuracy of oil-gas relative permeability from two-phase flow experiments." SCA - 9707, presented at the SCA Symposium. Calgary, Canada, 8-10 Sept. 1997.
12. Vatne, K.O.: :"Relative permeabiliteter og endepunktsmetninger som funksjon av kapillartallet," Hovedoppgave, Høgskolesenteret i Rogaland, Stavanger, 1988.
13. Virnovsky G.A., Skjaeveland S.M., Guo, Y.: "Relative permeability and capillary pressure concurrently determined from steady-state flow experiments." Presented at the 8th European Symposium on Improved Oil Recovery, Vienna, Austria 15-17 May 1995.
14. Virnovsky G.A., Guo, Y., Skjaeveland S.M., Ingsoy, P.: "Steady-state relative permeability measurements and interpretation with account for capillary effects." Presented at the SCA Conference held in San Francisco, USA, 12-14 Sept. 1995.
15. Virnovsky G.A., Skjaeveland S.M. Surdal, J., Ingsoy, P. "Steady-state relative permeability measurements corrected for capillary effects." SPE 30541, presented at the SPE ATCE held in Dallas, USA, 22-25 Oct. 1995.
16. Virnovsky, G.A. Mykkeltveit, J., Nordtvedt, J.E.: "Application of

a steady-state three-phase simulator to interpret flow experiments." SCA-9635. Presented at the SCA Symposium, September 8-10, 1996, Montpellier, France.

Appendix - Analysis of errors caused by end effects

Let us analyze the errors in relative permeabilities determined from steady state floods by Darcy's law, i.e., the errors caused by neglecting capillary forces. The analysis is based on implementation of equations (1) and (2).

Define 2 saturation values:

capillary limit saturation, S_{cl}, is the limiting (average) saturation in the core as total velocity tends to zero. This is the saturation value at which the capillary pressure curve (corresponding to the process in question) crosses the saturation axes. Capillary limit saturation depends on the capillary pressure curve, i.e., on the conditions at which the experiment is run (imbibition or drainage).

viscous limit saturation, S_{vl}, is the limiting (average) saturation in the core as total velocity tends to infinity. This saturation is completely defined by the fractional flow at injection, F (it is the solution of the equation $f(S_{vl})=F$), and therefore is a function of F, $S_{vl}= S_{vl}(F)$. Since relative permeabilities may also reveal hysteresis the viscous limit saturation is also dependent on the direction of the saturation change during the experiment.

Assign index 1 to the wetting phase (water), and index 2 to the non-wetting phase (oil). Consider two cases depending on whether viscous limit saturation is smaller or bigger then the capillary limit saturation.

Case A: $S_{vl}(F)<S_{cl}$

For water-wet rock, this case corresponds to primary drainage conditions for all F, and to imbibition and secondary drainage conditions for sufficiently low F.

The measured total pressure drop across the core corresponds to the 2-nd phase (oil), which means that the quantity of $\tilde{k}_{r2}$ is the measured relative permeability to oil.

It can be shown from the analysis of the equation describing steady-state 2-phase flow and corresponding boundary conditions that the saturation is increasing in the direction of flow, and average saturation is decreasing with total velocity increasing, i.e.:

$$\frac{dS}{dx} > 0, \quad \frac{dS}{du_t} < 0, \tag{8}$$

and therefore

$$S^0 < \overline{S} \tag{9}$$

We now show that

$$\tilde{k}_{r1}' = \frac{d\tilde{k}_{r1}}{du_t} < 0; \tag{10}$$

$$\tilde{k}_{r1}' = \frac{FL\mu_1}{k}\left(\frac{u_t}{\Delta p_1}\right)' = \frac{FL\mu_1}{k}\frac{\Delta p_1 - \Delta p_1' u_t}{\Delta p_1^2} \tag{11}$$

$$\Delta p_1 - \Delta p_1' u_t = u_t\left(\frac{\Delta p_1}{u_t} - \frac{F}{\lambda_1^0}\frac{L}{k}\right) = u_t\left(\frac{F}{k}\int_0^L \frac{dx}{\lambda_1} - \frac{F}{\lambda_1^0}\frac{L}{k}\right) =$$

$$= u_t \frac{FL}{k}\left(\frac{1}{L}\int_0^L \frac{dx}{\lambda_1} - \frac{1}{\lambda_1^0}\right) < 0$$

$$\lambda_1^0 = \lambda_1(S^0)$$

Similarly, it can be shown that

$$\frac{d\tilde{k}_{r2}}{du_t} > 0 \tag{12}$$

The total error is:

$$\Delta k_{ri}(\overline{S}) = \Delta\tilde{k}_{ri}(\overline{S}) - k_{ri}(\overline{S}) = \left[\Delta\tilde{k}_{ri}(\overline{S}) - k_{ri}(S^0)\right] + \left[k_{ri}(S^0) - k_{ri}(\overline{S})\right], \quad i = 1,2 \tag{13}$$

For the first phase, the first bracketed term in Eq. (13) is positive because of Eq. (10) and (3). The second bracketed term is negative because the saturation increases in the flow direction, i.e.:

$$\left[\Delta\tilde{k}_{r1}(\overline{S}) - k_{r1}(S^0)\right] > 0$$
$$\left[k_{r1}(S^0) - k_{r1}(\overline{S})\right] < 0 \tag{14}$$

Since the two terms will (partly) cancel out, no general conclusions can be drawn about the relative permeability to the 1-st phase.

For the second phase, the first bracketed term in Eq. (13) is negative because of Eq. (12) and (3). The second bracketed term is negative because the saturation increases in the flow direction. Thus the total error in the relative permeability to the 2-nd phase is always negative, $\Delta k_{r2}(\overline{S}) < 0$, i.e., the conventional interpretation of the measurements will underestimate relative permeability to the non-wetting phase.

Case B: $S_{vl}(F)<S_{cl}$

For water-wet rock, this case corresponds to imbibition and secondary drainage conditions for sufficiently high F.

The measured total pressure drop across the core corresponds to the 1-st phase (water).

Contrary to the previous case, in the case B the saturation is decreasing in the direction of flow, and average saturation is increasing with total velocity increasing. The analysis is performed similarly to the above one and gives the following conclusion:

The total error in the relative permeability to the 1-st phase is always negative, $\Delta k_r(\bar{S}) < 0$, i.e., the conventional interpretation of the measurements will underestimate relative permeability to the wetting phase.

TABLE 1 - FLUIDS' PROPERTIES

N	Viscosity at 30°C and 35 bar [cP]	Density at 30°C and 35 bar [g/ml]
Water	0.851	1.023
Oil	0.737	0.7197

TABLE 2 - CORE PROPERTIES

Core	Berea
Length [cm]	24.85
Diameter [cm]	3.78
Vp helium [ml]	56.14
Kw high rate test [mD]	165
Kw low rate test [mD]	208
Kw medium rate test [mD]	216

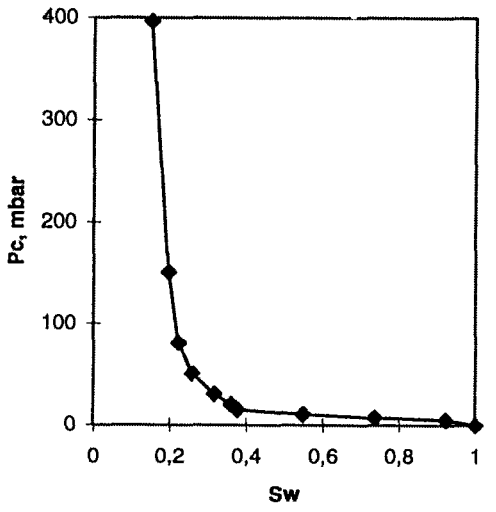

Figure 1. Primary drainage capillary pressure measured by centrifuge.

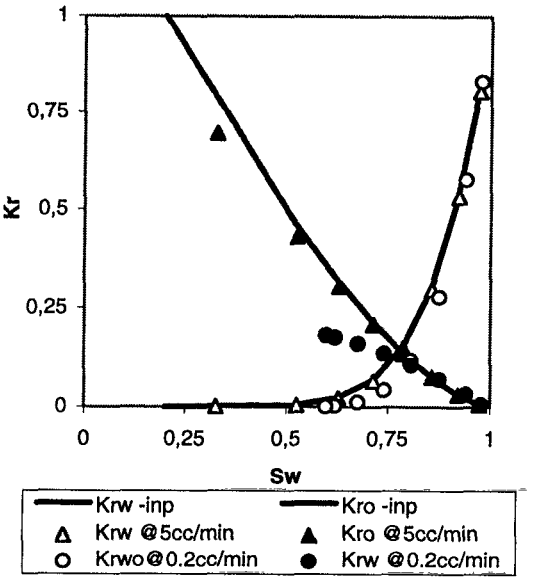

Figure 2. Relative permeabilities from simulated steady-state tests at rates 5 cc/min and 0.2 cc/min compared to the simulator input curves.

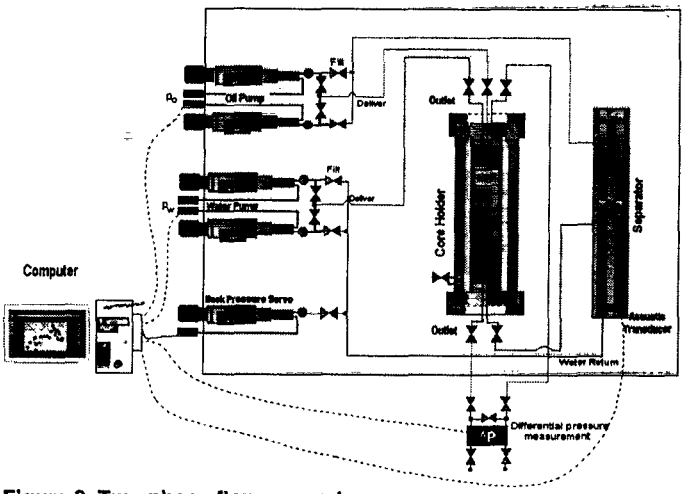

Figure 3. Two-phase flow apparatus

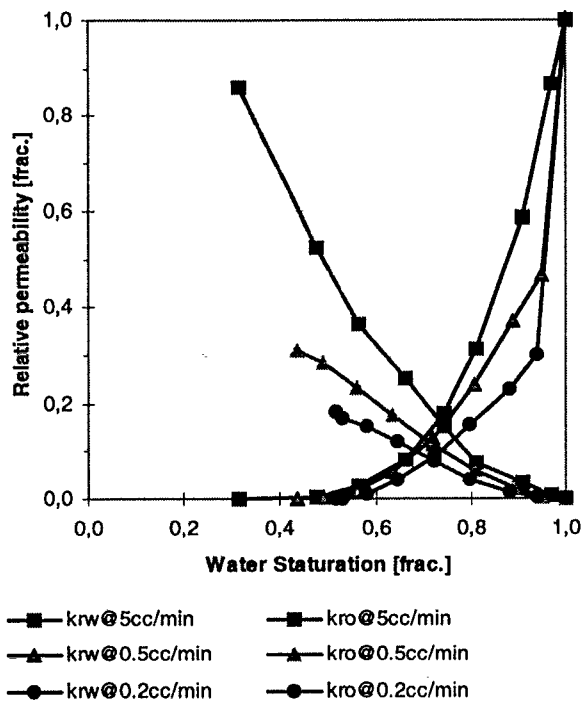

Figure 4. Relative permeabilities measured at three rates corrected for gravity.

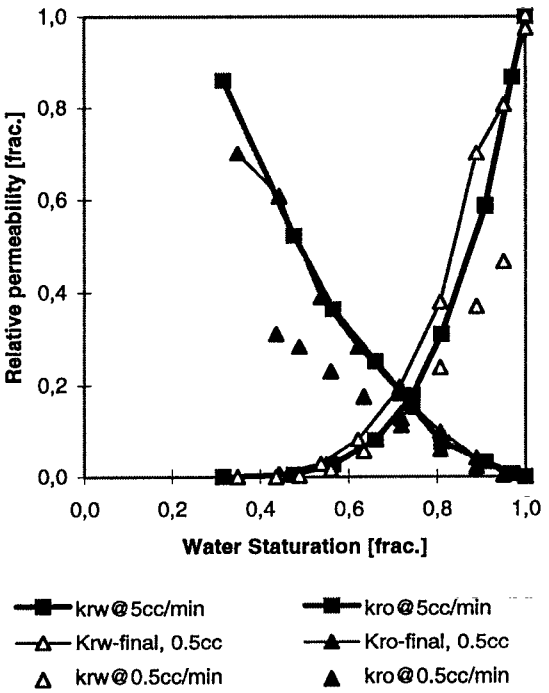

Figure 6. . Relative permeabilities measured at total rate 0.5 cc/min (triangles), with analytical corrections (triangles and circles), and measured at total rate 5 cc/min (lines and squares)

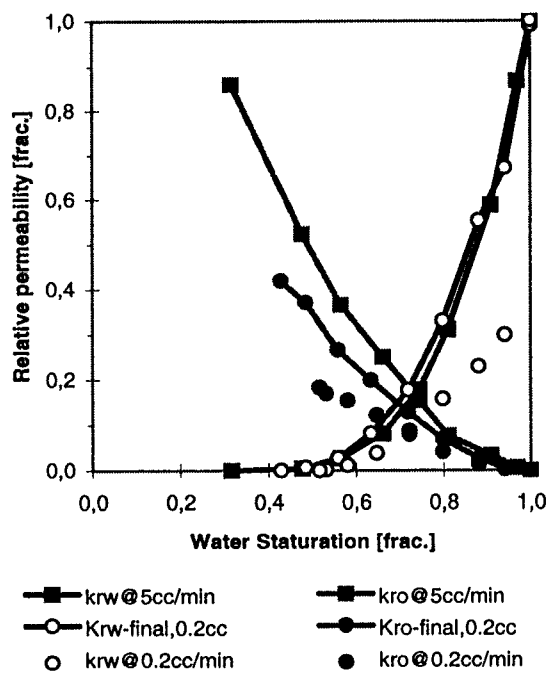

Figure 5. Relative permeabilities measured at total rate 0.2 cc/min (circles), with analytical corrections (lines and circles), and measured at total rate 5 cc/min (lines and squares)

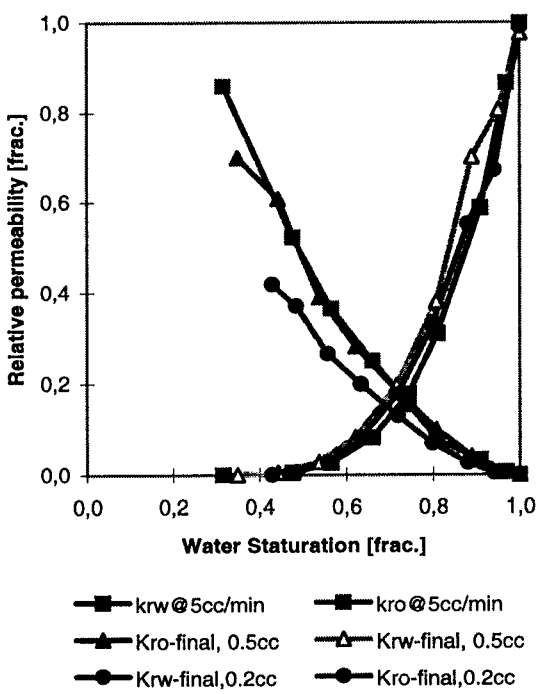

Figure 7. Relative permeabilities at total rate of 0.5 cc/min (triangles), and 0.2 cc/min (circles) with analytical corrections, and measured at total rate 5 cc/min (lines and squares)

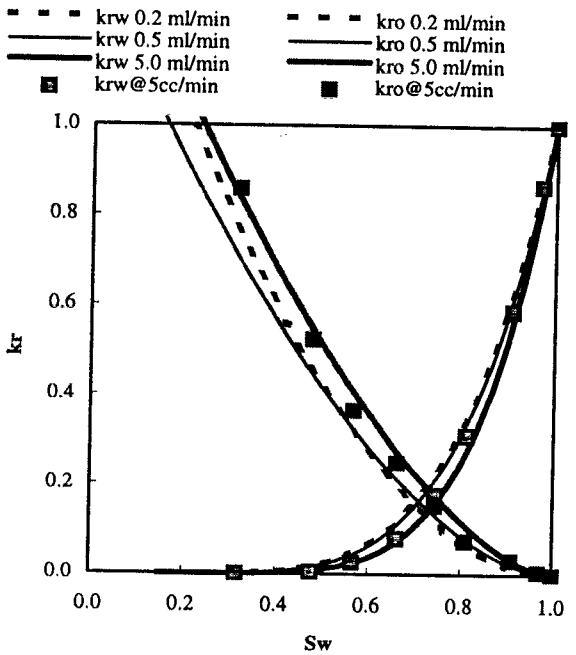

Figure 8. Relative permeabilities at three different rates from history matching (lines) and from Darcy interpretation of the high rate test (squares).

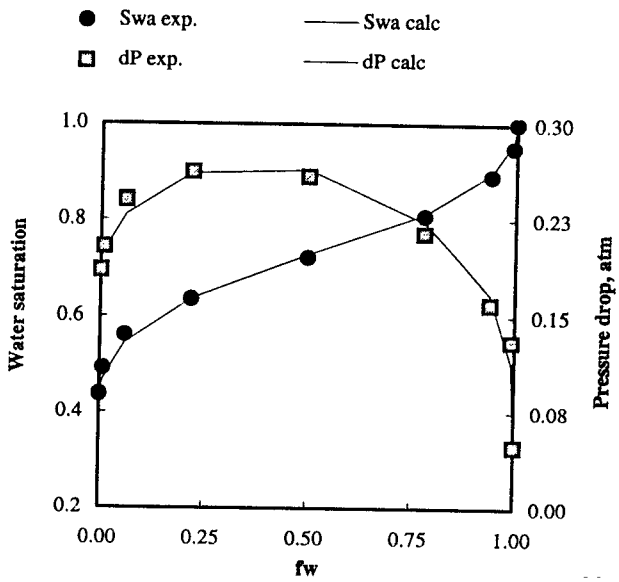

Figure 10. Measured and simulated average water saturation and pressure drop at total rate of 0.5 cc/min.

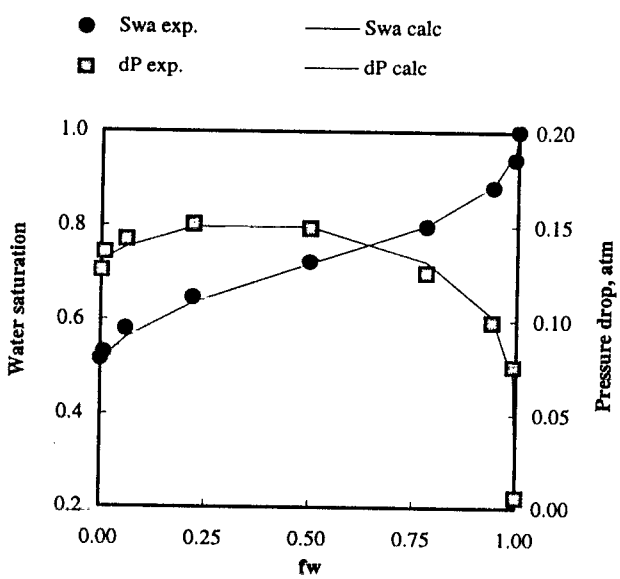

Figure 9. Measured and simulated average water saturation and pressure drop at total rate of 0.2 cc/min

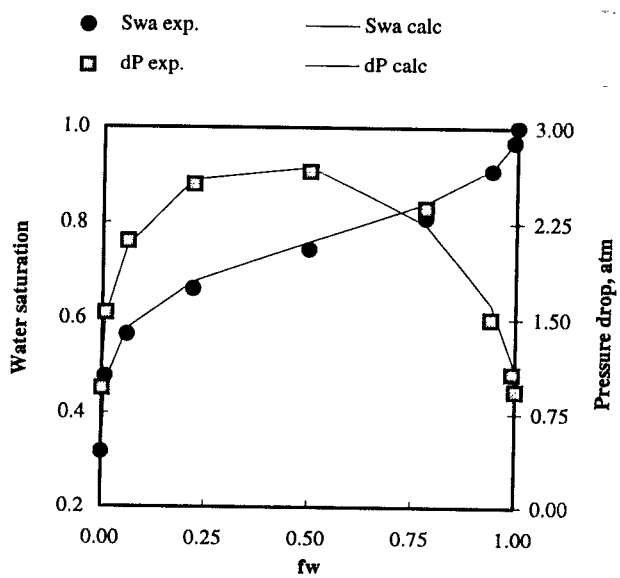

Figure 11. Measured and simulated average water saturation and pressure drop at total rate of 5 cc/min

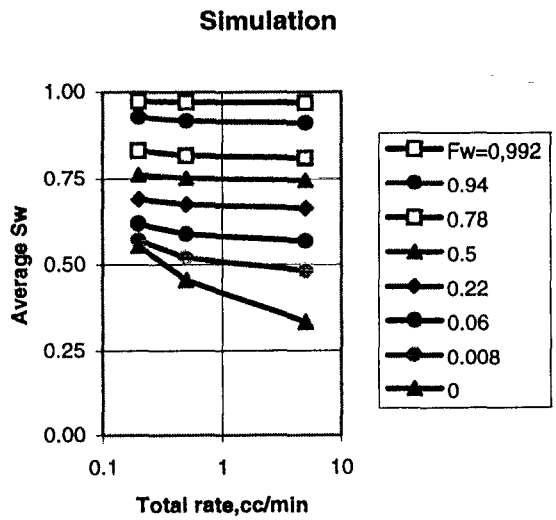

Figure 12. Rate dependence of average water saturation in the core from simulation runs.

Figure 13. Rate dependence of average water saturation in the core from experiments.

TABLE 3 - MEASURED DATA

Oil Fraction	Average Water Saturation			Pressure Drop, mbar		
	0.2cc/min	0.5cc/min	5cc/min	0.2cc/min	0.5cc/min	5cc/min
0.000	1.000	1.000	1.000	30.6	73.4	964
0.008	0.941	0.950	0.969	101.7	156.7	1103.7
0.060	0.880	0.889	0.909	125.7	186.7	1543.7
0.220	0.798	0.808	0.810	151.7	242.2	2418.7
0.500	0.722	0.719	0.744	175.7	286.7	2713.7
0.780	0.647	0.635	0.661	177.7	290.2	2608.7
0.940	0.581	0.560	0.565	169.7	268.7	2158.7
0.992	0.531	0.489	0.477	162.7	231.2	1588.7
1.000	0.517	0.437	0.316	152.7	212.7	979

TABLE 4 - CAPILLARY CORRECTION FOR SATURATION

Oil Fraction	Average Water Saturation		dS	dS/dln(q_t)	Water saturation at injection	
	0.2cc/min	0.5cc/min			0.2cc/min	0.5cc/min
0.000	1.000	1.000	0,000	0,00	1,000	1,00
0.008	0.941	0.950	0,000	0,00	0,941	0,95
0.060	0.880	0.889	0,000	0,00	0,880	0,89
0.220	0.798	0.808	0,000	0,00	0,798	0,81
0.500	0.722	0.719	0,003	0,00	0,719	0,72
0.780	0.647	0.635	0,012	-0,01	0,634	0,62
0.940	0.581	0.560	0,021	-0,02	0,558	0,54
0.992	0.531	0.489	0,042	-0,05	0,485	0,44
1.000	0.517	0.437	0,080	-0,09	0,429	0,35

TABLE 5. CORRECTION FOR RELATIVE PERMEABILITITES AT 0.5 CC/MIN

Sleft@ 0.5cc/min	$\tilde{k}_{ro}$ @0.5cc	$\tilde{k}_{rw}$ @0.5cc	dln $\tilde{k}_{ro}$	dln $\tilde{k}_{rw}$	$\tilde{k}_{ro}$ -final,0.5cc	$\tilde{k}_{rw}$ -final,0.5cc
1,000	0,0000	0,9910	0,0000	0,0135	0,0000	0,9767
0,950	0,0034	0,6460	-0,4017	-0,1828	0,0060	0,8070
0,889	0,0211	0,5193	-0,4453	-0,2385	0,0410	0,7020
0,808	0,0590	0,3204	-0,3742	-0,1452	0,0997	0,3808
0,716	0,1127	0,1736	-0,3545	-0,1058	0,1839	0,1963
0,622	0,1737	0,0811	-0,3539	-0,0171	0,2830	0,0826
0,538	0,2265	0,0273	-0,3848	-0,0240	0,3906	0,0281
0,443	0,2791	0,0062	-0,4956	0,0538	0,6079	0,0058
0,349	0,3067	0,0000	-0,5153	0,0000	0,7009	0,0000

TABLE 6. CORRECTION FOR RELATIVE PERMEABILITITES AT 0.2 CC/MIN

Sleft@ 0.2cc/min	$\tilde{k}_{ro}$ @0.2cc	$\tilde{k}_{rw}$ @0.2cc	dln $\tilde{k}_{ro}$	dln $\tilde{k}_{rw}$	$\tilde{k}_{ro}$ -final	$\tilde{k}_{rw}$ -final
1,00	0,0000	1,0044	0,0000	0,0135	0,0000	0,9899
0,94	0,0023	0,5381	-0,4017	-0,1828	0,0040	0,6722
0,88	0,0135	0,4091	-0,4453	-0,2385	0,0263	0,5531
0,80	0,0406	0,2771	-0,3742	-0,1452	0,0686	0,3293
0,72	0,0791	0,1562	-0,3545	-0,1058	0,1290	0,1766
0,63	0,1219	0,0797	-0,3539	-0,0171	0,1986	0,0812
0,56	0,1542	0,0267	-0,3848	-0,0240	0,2658	0,0274
0,49	0,1700	0,0065	-0,4956	0,0538	0,3703	0,0062
0,43	0,1832	0,0000	-0,5153	0,0000	0,4186	0,0000